Mon. Not. R. Astron. Soc. **000**, 000–000 (0000) Printed 3 September 1998 (MN LaTeX style file v1.3)

The interstellar and intrinsic polarizations of EZ CMa

T.J. Harries[1], I.D. Howarth[2], R.E. Schulte-Ladbeck[3], and D.J. Hillier[3]
[1] *Mullard Space Science Laboratory, University College London, Holmbury St. Mary, Dorking, Surrey RH5 6NT, UK*
[2] *Department of Physics and Astronomy, University College London, Gower Street, London WC1E 6BT, UK*
[3] *Department of Physics and Astronomy, University of Pittsburgh, 3941 O'Hara Street, Pittsburgh, PA 15260, USA.*

Dates to be inserted

ABSTRACT

We present multi-epoch, intermediate-dispersion linear spectropolarimetry of the pathological Wolf-Rayet star EZ CMa. The continuum polarization shows long-term quasi-periodic variations, both in polarization magnitude (range 0.8%) and position angle (60°), and we observe changes in the polarization vector at emission-line wavelengths. We argue that the interstellar polarization (ISP) can be estimated from the convergence point of continuum-to-line polarization vectors, and we find that the ISP at 5800Å is $0.47 \pm 0.02\%$ at a position angle of $164 \pm 2°$.

We subtract the new ISP estimate from our spectra to yield intrinsic polarized line-profiles of unprecedented quality. We discuss the characteristics of the profiles, and compare them with synthetic profiles computed using radiative-transfer codes. Measurements of the line profiles provides some evidence for ionization stratification in the wind.

The polarization variation produced by rotational modulation of an azimuthally structured wind is investigated by using a simple single-scattering model. An 'orange-segment' wind structure is capable of reproducing the amplitude of the observed polarization variations, although the shape of the polarized-light curve cannot be matched using a simple model.

Key words: Stars – Stars: early type – Stars: mass-loss – Stars: individual: EZ CMa – Polarization

1 INTRODUCTION

EZ CMa (HD 50896; WR 6 in the catalogue by van der Hucht et al. 1981) is one of the brightest Wolf-Rayet stars, and as such has, in many respects, become a prototype, particularly following the non-LTE modelling work of Hillier (1987a, 1987b, 1988). However, it is well known that the system exhibits unusual properties. In particular, extensive photometric and spectroscopic observations indicate variability with a 3.77-day period, although the detailed nature of the changes differs from season to season (e.g., McLean 1980; Cherepaschuck 1981; Lamontagne, Moffat & Lamarre 1986; van Genderen, van der Hucht & Steemers 1987; Robert, Moffat & Seggewiss 1991; Drissen et al. 1989, hereinafter D89; Willis et al. 1989; Robert et al. 1992; St-Louis et al. 1993; St-Louis et al. 1995; Antokhin et al. 1994; Duijsens et al. 1996; Morel, St-Louis & Marchenko 1997). While this periodic variability naturally leads to the suspicion that the WR star is the primary of a short-period binary, spectroscopic studies have failed to provide conclusive evidence for or against the system's binarity (e.g., St-Louis et al. 1993; Morel et al. 1997). However, the absence of easily detectable Keplerian radial-velocity variations in the WR emission-lines rules out a massive (10–20$M_\odot$) companion, while a compact secondary is expected to generate X-ray emission at levels 10–100 times greater than actually observed (Stevens & Willis 1988; Skinner, Itoh & Fumiaki 1997).

Spectropolarimetry of EZ CMa was first reported by McLean et al. (1979, hereinafter MC79). Their observations, spanning 3400–6000Å at 50-Å resolution, showed that all the prominent spectral lines are depolarized with respect to the continuum. Since the continuum radiation is formed at smaller radii than the line emission, and therefore 'sees' greater electron-scattering optical depth in the wind, this behaviour can be broadly understood in terms of an asymmetric distribution of scatterers; however, MC79 found that the polarization decreases across the lines could not be adequately modelled by simple dilution, and suggested that ionization stratification could explain the polarization spectrum, with the lines of more highly ionized species being produced deeper in the wind and hence undergoing more electron scattering. In addition, they noted that the rapid variations observed in the polarization implied non-steady mass-loss in an envelope which is not axisymmetric.

Schulte-Ladbeck et al. (1990, 1991, hereinafter SL90 and SL91 respectively) presented further low-resolution (~34-Å fwhm) polarization spectra, confirming that the polarization vector changes across the line wavelengths. The He II λ4686 emission line was shown to trace a loop in QU space, behaviour previously observed in Be stars (Poeckert & Malborough 1978) and in SN 1987A (Cropper et al. 1988). SL90 noted that the polarization minimum of the emission line was redshifted with respect to the flux maximum, and suggested that the polarization was a result of electron scattering in a rotating, expanding axisymmetric disk structure. They also investigated the use of emission-line polarization as a diagnostic of the ionization stratification in the wind. Robert et al. (1992) published medium-resolution spectropolarimetry which also showed line-depolarization and QU loops for the λ5412 He II emission line, although the sense of the loops changed during their observing session.

In spite of the extensive observational effort which has been expended on EZ CMa, a number of basic questions remain unresolved. Is the system single or binary? What is the extent of foreground polarization, and what are the implications for inferences regarding the intrinsic polarization? Can spectropolarimetry effectively be exploited as an ionization-stratification diagnostic? To attempt to address these questions, we have collected linear spectropolarimetry of EZ CMa on a number of occasions, sampling a variety of timescales, with higher spectral resolution than in previous observations.

2 OBSERVATIONS AND DATA REDUCTION

Observations were obtained with the RGO spectrograph on the 3.9-m Anglo-Australian Telescope (AAT), equipped with a polarimetry unit consisting of a rotating half-wave plate modulator and a calcite analyzer. A journal of the observations is given in Table 1.

Standard polarimetric observing procedures were adopted, with four exposures (corresponding to the 0°, 22.5°, 45°, and 67.5° positions of the half-wave plate) constituting one observation. A two aperture dekker (apertures A and B) was employed (one aperture for the target and one for sky background), and the star was typically observed in the sequence A-B-B-A. Preliminary data reduction, including bias subtraction and cosmic-ray cleaning, was performed by using the FIGARO package (Shortridge et al. 1996). Polarimetric reduction was performed using the methods described by Harries & Howarth (1996), and subsequent analysis conducted with POLMAP (Harries 1996). Observations of polarized standard stars were used to calibrate the position-angle (PA) zero-point while observations obtained through a 100%-polarizing filter were employed to remove the small PA–wavelength dependence introduced by the slight chromacity of the half-wave plate. The instrumental polarization, estimated from unpolarized standards, was less than 0.1%. Spectra taken on the same night were then summed to produce nightly mean polarization spectra.

Table 1. A summary of the observations of EZ CMa. The dates of observation are listed, along with the photometric phase (according to Equation 1), the central wavelength, the reciprocal dispersion, and the number of polarimetric observations (N). (Where one observation consists of integrations at each of the 4 half-wave plate settings.)

Date	HJD −2400000	ϕ	$\lambda_{\rm cen}$ (Å)	$\Delta\lambda$ Å pix^{-1}	N
1991 Jan. 28	48285.146	0.995	5580	1.1	68
1991 Jan. 29	48286.026	0.228	5580	1.1	26
1992 March 11	48692.011	0.296	4960	1.1	44
1992 March 12	48692.980	0.031	4960	1.1	16
1992 March 17	48698.925	0.867	6560	0.6	4
1994 May 6	49478.871	0.969	6580	0.7	8
1994 May 7	49479.847	0.228	6580	0.7	12
1994 May 8	49480.851	0.494	6580	0.7	12
1994 May 9	49481.856	0.761	6580	0.7	10
1995 Apr. 28	49836.370	0.897	6560	0.7	8
1995 Apr. 28	49836.292	0.876	4686	0.7	4
1995 Apr. 29	49837.402	0.171	6560	0.7	4
1997 Aug. 9	50670.825	0.473	6560	0.7	4

2.1 The polarization spectra

A montage of all our observations of EZ CMa is presented in Figure 1. The range in continuum polarization is 0.8%, while the position angle of the polarization varies over a range of 60°; these are close to the extreme ranges recorded in the extensive photopolarimetry reported by D89.

The changes in the polarization vector through the emission lines, first noted by MC79, are also clearly present in these observations. The magnitude of the polarization generally decreases through the emission line, but for one observation (λ6560 on 6$^{\rm th}$ May 1994) the magnitude of the polarization is *larger* at the emission-line wavelength. It is noteworthy that the polarization vectors are more nearly constant in the lines than the continuum, particularly for the strongest lines, such as λ4686 and λ6560. This observation is consistent with the narrow-band (~ λ4686) photopolarimetry of Moffat & Piirola (1993).

2.2 Phase dependence

The continuum polarization of each spectrum was calculated by summing the Stokes parameters over the entire spectrum, excepting regions containing obvious emission lines. The phase of each observation was obtained from the mid-times of exposure and the ephemeris given by Lamontagne, Moffat & Lamarre (1986), based on long-term photometric monitoring:

$$\mathrm{HJD}\,2446153.61 + 3.766E, \tag{1}$$

where phase zero corresponds to the time of maximum light (1980–85). The resulting normalized Stokes parameters are plotted as a function of phase in Figure 2.

The observed continuum variations are broadly consistent with the photopolarimetry reported by Robert et al. (1992). Since the shape of the polarized light-curve is known to vary on a timescale of months, the differences between the

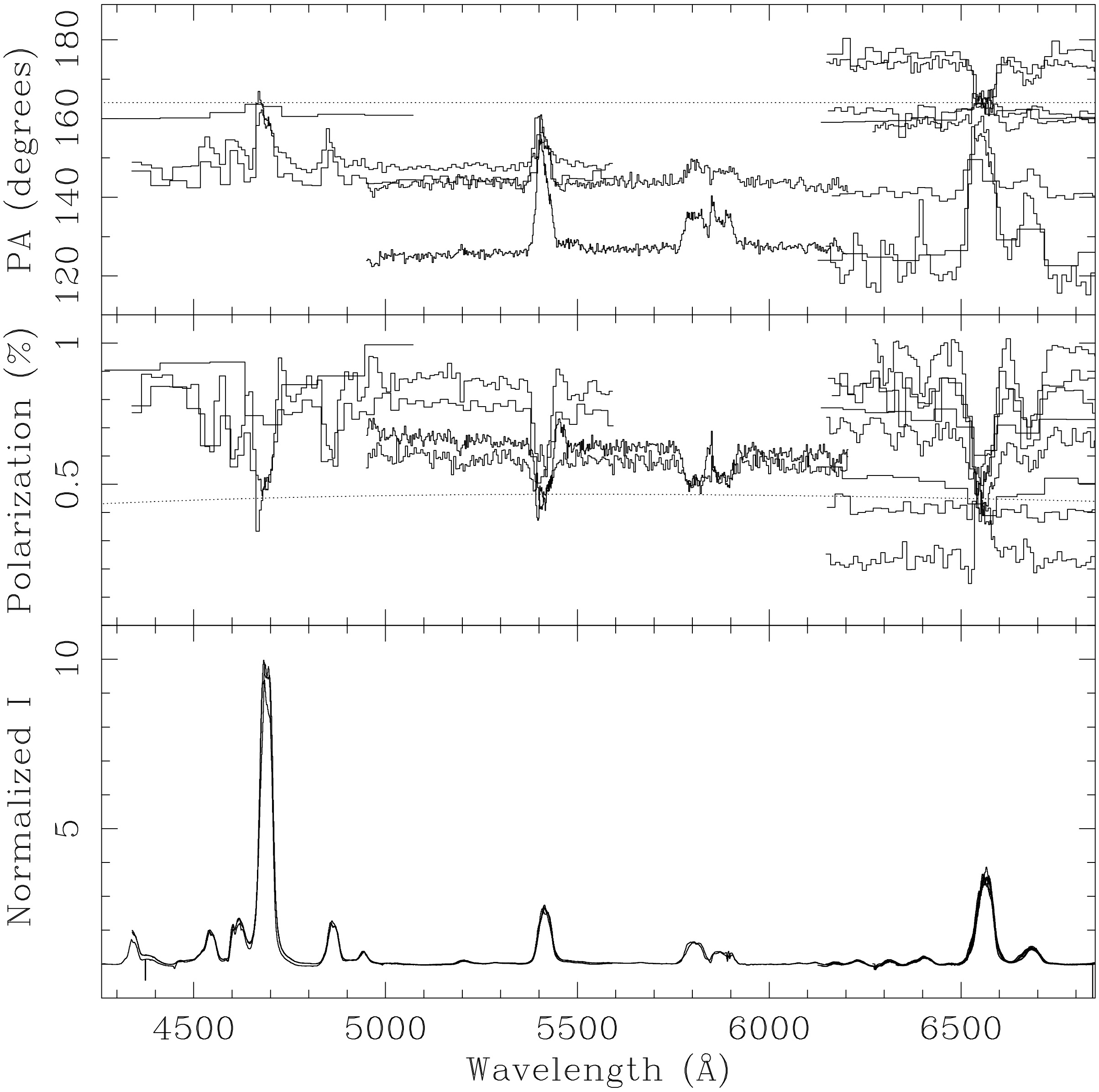

Figure 1. A combined plot of all observations of EZ CMa. The data from 1991 Jan. (4340–5590Å), 1992 March (4950–6205Å), 1994 May (6150–6960Å), 1995 April (4260–5080Åand 6130–6950Å), and 1997 August (6130–6950Å) are all binned to a constant error of 0.02% in polarization. The dotted line represents the ISP law discussed in §3.

five sets of observations (1991 Jan., 1992 March, 1994 May, 1995 April, 1997 August) are not surprising.

3 THE INTERSTELLAR POLARIZATION

Interstellar polarization (ISP) is the result of dichroic absorption by aspherical dust particles aligned in the Galactic magnetic field. The ISP reaches a maximum in the optical region and is usually well modelled by the empirical Serkowski law,

$$P(\lambda) = P_{\max} \exp[-k \ln^2(\lambda_{\max}/\lambda)] \tag{2}$$

(Serkowski 1973), where $P_{\max}$ is the maximum polarization, occuring at a wavelength $\lambda_{\max}$, and k is a shape parameter (normally $\sim$1.15).

Several previous estimates of the ISP to EZ CMa have been reported in the literature. MC79 combined $p \simeq 1.67 A_V$

Table 2. Polarization measurements of EZ CMa. The polarizations are given as percentages. The one-sigma error on the polarization measurements is 0.02%.

Date	q_c	u_c	q_ℓ	u_ℓ
		He II/H Iλ6560		
1992 March 17	+0.743	−0.638	+0.437	−0.290
1994 May 06	−0.199	−0.193	+0.226	−0.296
1994 May 07	+0.642	−0.144	+0.352	−0.234
1994 May 08	+0.691	−0.545	+0.507	−0.294
1994 May 09	+0.399	−0.036	+0.381	−0.215
1995 Apr. 28	+0.554	−0.482	+0.453	−0.348
1995 Apr. 29	−0.236	−0.480	+0.151	−0.348
1997 Aug. 9	+0.149	−0.818	+0.359	−0.354
		He II λ5412		
1991 Jan. 28	+0.380	−0.798	+0.406	−0.441
1991 Jan. 29	+0.266	−0.739	+0.338	−0.423
1992 March 11	−0.226	−0.625	+0.234	−0.387
1992 March 12	+0.172	−0.584	+0.295	−0.332
		He II λ4686		
1991 Jan. 28	+0.366	−0.768	+0.382	−0.310
1991 Jan. 29	+0.239	−0.744	+0.368	−0.334
1995 Apr. 28	+0.782	−0.630	+0.591	−0.418

(Serkowski, Mathewson & Ford 1975) with a reddening estimate of $A_V = 0.25$ to obtain a polarization of 0.25%, and used the polarization properties of field stars to estimate the position angle as 35°. SL90 fit a Serkowski law to the continuum polarizations in several spectropolarimetric observations and the direction of their line polarizations, obtaining $P_{\rm max} = 0.55\%$ at PA 0°. SL91 re-examined the ISP, using a least-squares fit of a Serkowski law to multi-epoch observations of EZ CMa; this resulted in a $P_{\rm max} = 0.58\%$ at 176°. In addition, they examined the polarizations of 10 nearby field stars, finding an average of 0.19% at 31° (in reasonable agreement with McLean et al.). Robert et al. (1992) estimated an interstellar polarization of 0.5% at 160° from their spectropolarimetric observations. Thus the field-star method yields an ISP that is very different from the value derived from a simple analysis of the observed polarization spectrum.

An approximate value of the ISP can be estimated directly from the observations presented in Figure 1. Since the polarization of λ6560, in particular, remains remarkably constant in spite of large-scale continuum variability, it is evident that the *intrinsic* line polarization is close to zero, so that the *observed* line polarization is almost entirely interstellar. From these considerations we can make a preliminary estimate of the ISP as 0.4% at 160°. We can improve on this estimate, however, by using all the information present in the observations. To do this, we measured polarizations (in QU space) over the emission lines (q_ℓ, u_ℓ) and in adjacent line-free continuum bins (q_c, u_c; 6760–6820Å for λ6560; 5080–5120Å for λ5412; and 5000–5040Å for λ4686). The emission-line bins were 10Å wide, centred on the central wavelength. The results are summarized in Table 2.

Figure 3 shows a schematic diagram of the polarization vectors under consideration. The observed continuum polarization ($0C$) is the vector sum of the interstellar polarization vector ($0I$) and the intrinsic continuum polarization (IC). The diluting unpolarized line flux means that the polarization in the line (IL) is some fraction of the continuum polarization, giving an observed line polarization $0L$. If some of the line flux is polarized, but in the same direction as IC, then the vector IL is still colinear with IC. (This is always the case in axisymmetric systems, but can also be true in a wide variety of more complex geometries.) Under these circumstances, the vector joining the head of continuum polarization to the head of the line polarization will lie in the direction of the head of the interstellar vector, $0I$. This argument is valid even when the background source shows polarization variability; indeed, such variability is essential to produce a well-defined convergence point.

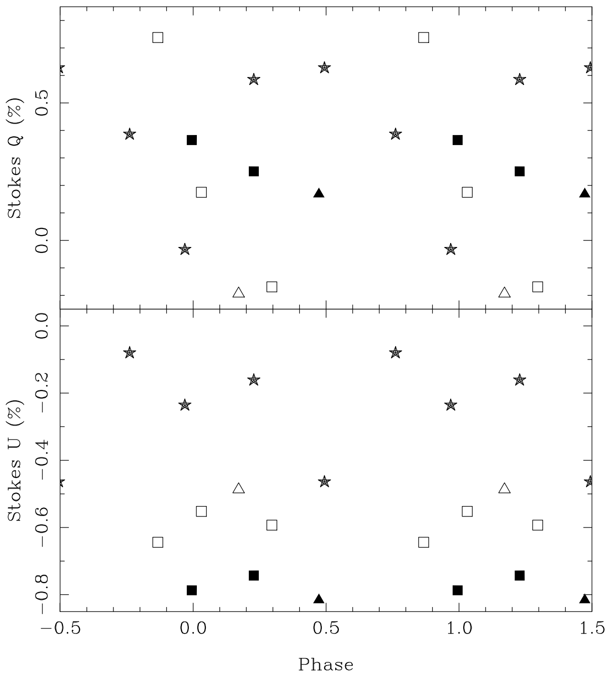

Figure 2. The continuum polarization of EZ CMa as a function of the 3.77-day period; formal errors are less than 0.01%. The data shown are from 1991 Jan. (filled squares), 1992 March (open squares), 1994 May (stars), 1995 April (open triangles), and 1997 August (filled triangles).

Figure 4 gives the polarization 'colour' diagram of the vectors summarized in Table 2. Although the ISP will have some wavelength dependence, over the relatively small range of our observations the head of the ISP vector can be considered as a point in the QU plane, and the diagram clearly shows that the colour vectors have a well defined convergence point. The ISP derived by MC79 from the field-star method is outside the convergence zone of these observations, as is that reported by SL91.

The mean polarization of our line measurements is $q = Q/I = 0.35\%$, $u = U/I = -0.32\%$ (0.47% at 159°), but clearly not all the lines are completely depolarized. A more robust method of ISP estimation is to find the point in the QU plane at which all the continuum-to-line polarization vectors point, which assumes only that the line and continuum photons are scattered in the same geometry. To

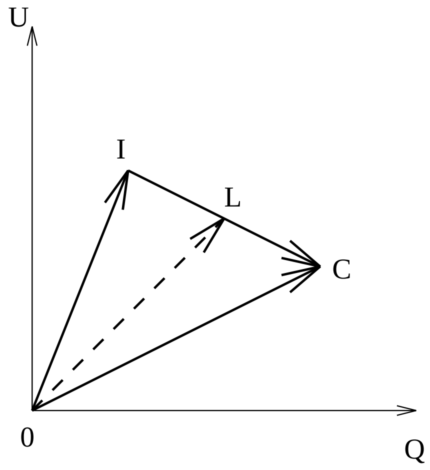

Figure 3. A schematic diagram showing the relationship between the observed continuum polarization (OC), the observed line polarization (OL), and intrinsic (IC) and interstellar (OI) polarization.

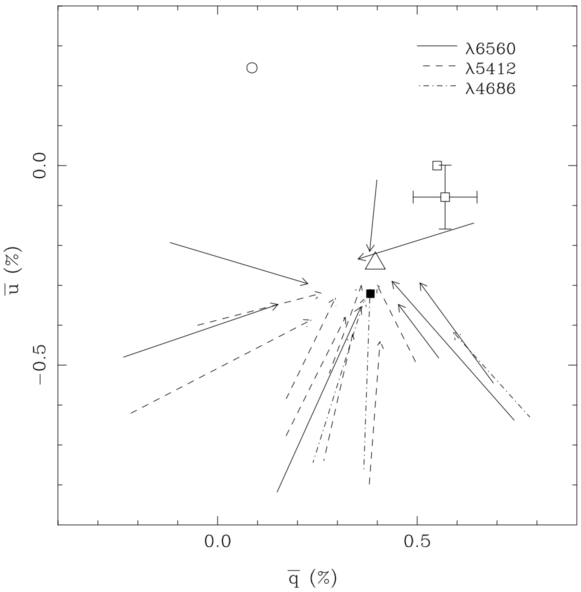

Figure 4. The polarization 'colour' vectors. The continuum polarizations are joined to the line polarizations, with the arrowheads pointing to the line polarizations. Data are taken from Table 2 and from the AAT spectropolarimetry of Robert et al. (1992). The ISP values estimated by MC79 (open circle), SL90/SL91 (open squares) and Robert et al. (1992; filled square) are shown, along with the ISP derived in this study (open triangle). Colour vectors are shown for the λ6560 line (solid lines), the λ5142 line (dashed line) and the λ4686 line (dot-dashed line).

do this we perform at least-squares minimization of a line that passes through an assumed ISP, (q_i, u_i), through the continuum polarization, and through the line polarization. We then calculate a measure of goodness of fit,

$$\chi^2 = \frac{u_\ell - u_i - b(q_\ell - q_i)^2}{\sigma^2_{u_\ell} + b^2\sigma_{q_\ell}} + \frac{u_c - u_i - b(q_c - q_i)^2}{\sigma^2_{u_c} + b^2\sigma_{q_c}}, \qquad (3)$$

where σ_{q_ℓ}, σ_{q_c}, σ_{u_ℓ}, σ_{u_c} are the errors on the normalized Stokes parameters for the line and continuum, and b is the gradient of the straight-line fit. The values of χ^2 are summed over all line–continuum polarization pairs, yielding a cumulative χ^2 for a given (q_i, u_i). By minimizing $\Sigma\chi^2$ we obtain a best estimate of (q_i, u_i); the minimization is performed by traditional numerical techniques (in our case with a downhill simplex).

We estimated errors on the (q_i, u_i) fit by Monte-Carlo simulations. The original dataset was perturbed by random Gaussian deviates with a standard deviation of 0.05%. [The errors on the polarization measurements in Table 2 (0.02%) are derived assuming photon-statistics, and represent a lower limit on the true errors. Experience has shown that the instrumental calibration can only be performed to an accuracy of 0.02–0.03% (Harries & Howarth 1996). Although imperfect instrumental offset calibration will lead to a *systematic* error for measurements taken during one observing session, we make the pragmatic assumption that the offset varies in a random fashion from session to session, and adopt a normal error of 0.05% on each line and polarization measurement.] The ISP value was then found, and the process repeated. After 1000 minimizations the mean ISP and its variance were calculated.

Using this method we find $q_i = 0.40 \pm 0.02$, $u_i = -0.25 \pm 0.03$ (see Figure 4), i.e., $P = 0.47 \pm 0.02\%$ at $164 \pm 2°$. We may take these values to apply at 5800Å, the mean wavelength of the lines used to derive the ISP, weighted by the number of line and continuum polarization measurements of each line. We recognise that the ISP will vary over the range 4686Å to 6560Å, and that this will introduce an additional, small ($\sim$ 0.01%) uncertainty on our ISP estimate. The rms of the minimum distances of the ISP point to the lines defined by the continuum and line polarization measurements is 0.03%, confirming the Monte-Carlo result.

This new estimate of the ISP is inconsistent with that of MC79, but is just consistent (at the 2σ level) with the ISP derived by SL91 ($P = 0.58 \pm 0.08\%$ at $176 \pm 4°$), and is in excellent agreement with that derived by Robert et al. (1992).

4 THE INTRINSIC POLARIZATION SPECTRUM OF EZ CMA

The ISP law may be subtracted from the observations to yield the intrinsic polarization spectrum. To account for the wavelength dependence of the interstellar polarization we used a canonical Serkowski law with $k = 1.15$ and $\lambda_{\rm max} = 5500$Å (the results are insensitive to the precise values adopted given the relatively small wavelength range under consideration). Results are shown in Fig. 5.

The λ4686 and λ6560 lines are almost completely unpolarized in the intrinsic spectrum, resulting in the large uncertainty in the PA at these wavelengths. All the lines now

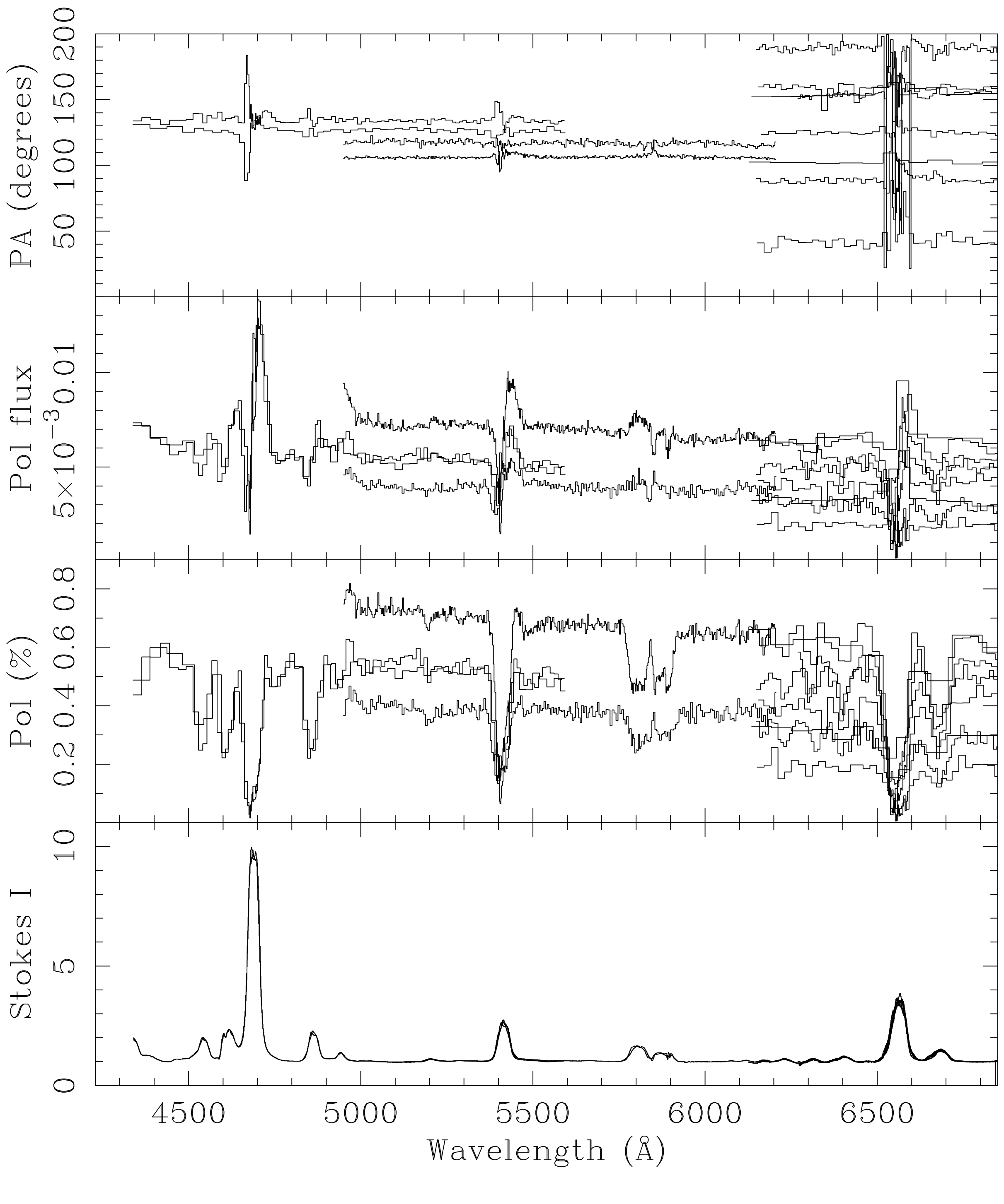

Figure 5. The ISP subtracted polarization spectra of EZ CMa. The observations of Jan. 1991, March 1992 and May 1994 are binned to a constant error of 0.02%

show a depolarization, including the 6th May 1994 observation which, in the uncorrected spectrum, had an apparent polarization *enhancement* at $\lambda6560$ due to the alignment of the intrinsic and ISP vectors. Most of the emission lines show a striking P-Cygni type structure in polarized flux (see §4.1).

The intrinsic polarization spectrum is flat to first order. This result is expected for pure electron scattering, since this is a grey process. There is some evidence for a mild decrease in the polarization spectrum to the red, particularly in the 11th March 1992 observation (largest polarization magnitude spectrum in Fig. 5), a result that is insensitive to the adopted value of $\lambda_{\rm max}$. A similar trend was noticed by SL91 in one of their low-resolution observations, and has also been reported for WR 134 (e.g., Schulte-Ladbeck et al. 1992). In principle, it can be attributed to increasing free-free optical depth with increasing wavelength, so that the red continuum is formed at larger radii than the blue continuum (and so undergoes less electron scattering), although simple estimates suggest that this effect should be small over the wavelength range considered here.

The range in intrinsic continuum polarization is approximately 0.2–0.7%, with a remarkable variation in PA of over 80° (note the 180° ambiguity in PA), although the PA is essentially constant as a function of wavelength for a given observation. This enormous range in PA clearly emphasizes that the greater part of EZ CMa's continuum polarization cannot originate in any stable axisymmetric structure, such as a disk.

4.1 The polarized line profiles

The combination of high signal-to-noise and an accurate ISP estimate yields excellent intrinsic polarized line profile observations, which may be compared with the predictions of the radiative-transfer models. We have plotted (unbinned) the best observed line profiles in Figure 6.

It is immediately apparent that there are polarization characteristics common to strongest emission lines:

The polarization magnitude shows a decrease from the blue wing, and the minimum polarization is generally reached before maximum line intensity (this is particularly evident for $\lambda5412$ and $\lambda6560$). The slope of the polarization magnitude with wavelength appears to be less steep on the red side of the profile. There is weak evidence enhancement in the polarization magnitude (compared to the continuum level) in the red wing of $\lambda5412$, and $\lambda4945$, but most lines show *no increased polarization magnitude in the red wings.*

The polarized flux shows a P Cygni-type profile for the majority of the lines. The emission component of this P Cygni structure is highly redshifted, for example an increase in polarized flux over the continuum level can be detected out to 5470Å for $\lambda5412$ (a velocity of over 3000km s^{-1}). The exception is the C IV $\lambda5801$–12 blend, which shows no absorption dip and polarized line emission that is less red-shifted than the other profiles (even allowing for the blend with the He I line). It is possible that the polarigenic mechanism in this line is not primarily electron-scattering. [The radiative transfer models suggest that this line is formed by continuum fluoresence (Hillier 1988), in which UV photons are absorbed in the $2s$–$3p$ transition at 312Å, and are re-radiated in the $3p$–$3s$ transition.]

The PA at the centres of the depolarized emission-lines is general ill-defined (since $\sigma_\theta \propto 1/P$), but there are apparently some small but significant variations in PA through some of the emission lines, which are likely to be due to small errors in the ISP estimate. The mean PA difference between the line and continuum measurements is $4.4 \pm 3.6°$, and it appears that the lines do not have a systematically different PA to the continuum. A variation in PA through the lines could arise physically if the line flux scatters in a different geometry to the continuum. This scenario is plausible if the global wind geometry close to the electron-scattering surface varies ($\tau_{es} = 1$) on timescales shorter than the flow time to the line-forming region; for example, according to the model of EZ CMa computed by Crowther (1994), the $\tau_{\rm es} = 1$ boundary lies at $\approx$5R$_*$, and the peak $\lambda4686$ line flux formation occurs at about 25R$_*$, giving a flow-time of about 6.5 hours (for $v \simeq v_\infty = 1700$ km s^{-1}). This is indeed smaller than the polarization variability time-scale; however, if this were consistently important then the dominant timescale of polarization would be this shorter one, rather than the 3.77-d period. Scattering in a rotating wind may also lead to systematic changes in PA through an emission line, with the polarization vectors tracing out a loop in the QU plane, and these loops have been observed in Be stars (Poeckert & Marlborough 1978) and SN1987A (Cropper et al. 1988). SL90 presented observations of the He II $\lambda4686$ emission line of EZ CMa, which clearly show a QU loop. None of the emission line observations presented here show QU loops, but rather trace a linear pattern in the QU plane. The difference between the two sets of observations once again point to a scattering geometry that is highly variable.

4.2 Model line polarization spectra

Model spectra of $\lambda5412$ and $\lambda4945$ were computed using a polarized radiative-transfer code (Hillier 1996). The emission-line source functions were computed using the non-LTE radiative transfer code of Hillier & Miller (1998) with R=2.5R$_\odot$, $v_\infty = 2000$km s^{-1}, $\dot{M} = 2.5 \times 10^{-5}M_\odot$ yr^{-1} and $L = 3 \times 10^5$L$_\odot$. The wind was clumped with a filling factor of 0.1, and the latitude dependency of wind density was $f(\mu) = 1.304(1 - 0.7\mu^2)$ where $\mu = \cos\theta$ and θ is the co-latitude. This structure was selected in order to approximately match the observed continuum polarization, and the models do not represent a fit to the data, but are presented for illustrative purposes.

The $\lambda5412$ model (Figure 7a) displays most of the characteristics that are observed. The polarization magnitude shows a sharper decline in the blue line-wing than the red, and the minimum magnitude occurs bluewards of the peak line intensity. The polarized flux shows a P Cygni structure, and of course the PA shows no variation through the line (the model is axisymmetric). The most striking difference between the model and the observation is the strength of the polarized red wing. It was noted in the previous section that there was no evidence for an extended red wing of polarization magnitude in the majority of lines, and only very weak evidence of a polarization magnitude enhancement in $\lambda5412$. Such a wing is clearly present in the model (despite

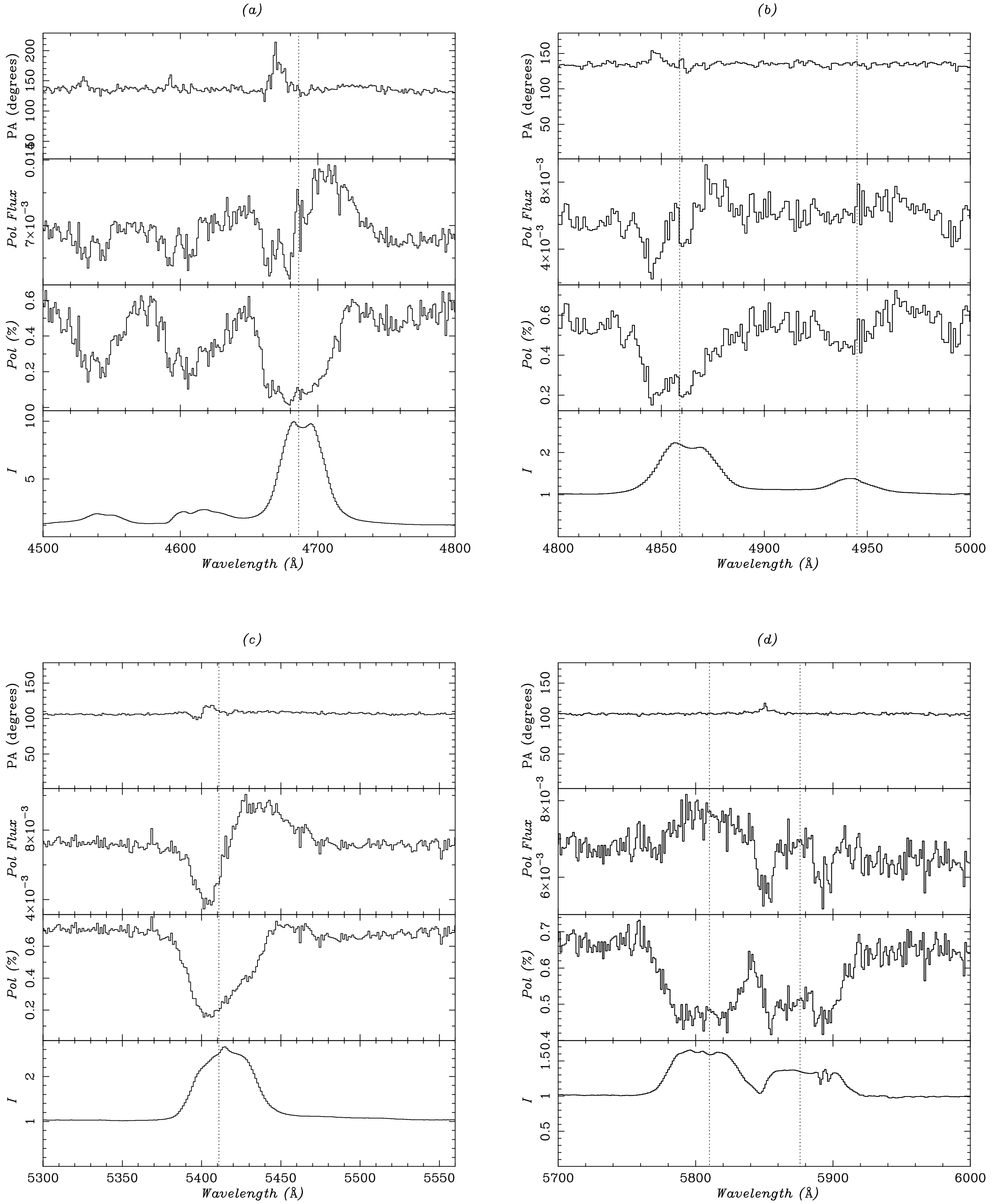

Figure 6. The intrinsic line profiles of EZ CMa: (a) He II $\lambda4686$, (b) He II $\lambda4859$ and N V $\lambda4945$, (c) He II $\lambda5412$, and (d) C IV $\lambda5801$–12 and He I $\lambda5876$. The dotted line shows the rest wavelength of the emission line. Note the P-Cygni form of the polarized flux profile, with the emission component strongly redshifted.

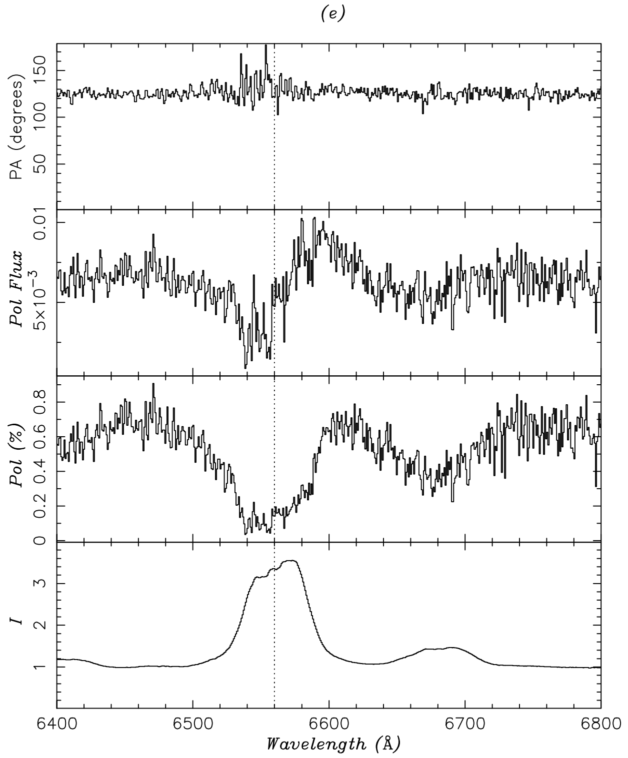

Figure 6. (concluded). The intrinsic line profiles of EZ CMa: (e) He II λ6560.

the inclusion of clumping), with a maximum polarization magnitude of about 0.3% above the continuum level.

The N V λ4945 emission line is produced at greater depth in the wind, and we therefore expect a greater line polarization. The model is in broad agreement with the (relatively poor) observation, which shows no P-Cygni profile in polarized flux and only a slight line depolarization.

The P Cygni structure of the polarized flux spectrum originates from a combination of line absorption and electron scattering. Electron-scattering in an expanding atmosphere leads to a nett redshift (the expanding universe paradigm), and the redshifted P Cygni emission component results from electron-scattering of line photons as they leave the wind. The absorption component results from absorption by the line of polarized continuum photons. Generally speaking a line produced deep in the wind will have a stronger emission component, and an optically thick line will have a strong absorption component. We therefore see a well-defined P Cygni structure for the He II lines, while the N V λ4945 line, which is formed deeper in the wind, shows only an emission component in polarized flux.

4.3 Line polarization measurements

The dominant mechanism that produces the line depolarization is dilution, although there is evidence for increased polarized line flux on the red-side of the profile (see Figure 6 and §4.1). In order to quantify this second-order effect we define a line polarization diagnostic:

$$R = \frac{\mathrm{EW}_{pf}}{\mathrm{EW}_{lf}} \tag{4}$$

where EW_{pf} is the equivalent width of the polarized line flux (measured from the line centre to the red edge of the red-wing), and EW_{lf} is the equivalent width of the emission line flux. Hence a large value of R indicates a line in which the line photons themselves are significantly polarized.

We measured the quantity R for all the strong emission lines in the dataset (errors were estimated from repeated measurements). We note that most measurements, excepting those for λ5412 are affected by line blends, and that the measurements of λ5876 were affected by the presence of the interstellar NaD doublet. The results are listed in Table 3.

Examining the mean values of the R parameter (see Table 4) we find broad evidence of ionization stratification. The mean average values for the species have R(N V)> R(He II)> R(He I), although λ4601–20 N V (which has blending problems with λ4686) and λ4859 He II (which is relatively weak) do not follow this general trend. The C IV blend has an R value of $+0.01 \pm 0.02$, consistent with the continuum fluoresence line formation mechanism (see §4.1).

The values of R for individual lines observed at different epochs show statistically significant variations (see Table 3), which implies that the depth of line formation or the electron-scattering optical depth to the observer is changing with time.

We measured R for the two models presented in Figure 7, and obtained $R(5412) = 0.51 \pm 0.02$ and $R(4945) = 1.09 \pm 0.02$). Both values are far in excess of mean observed values (0.239 ± 0.008 and 0.262 ± 0.154 for λ5412 and λ4945 respectively). Once again we can attribute this difference to the over-strong electron-scattered red-wings of the models.

5 THE NATURE OF THE CONTINUUM POLARIZATION VARIABILITY

Photopolarimetric observations provide one of the strongest lines of argument in favour of a binary model for HD 50896, showing phase-locked behaviour with the 3.77-d period (McLean 1980; D89; Robert et al. 1992). The polarization curve has a double-wave form, as expected for close binaries, but the durations and amplitudes of the two waves vary from epoch to epoch. By assuming an extended version of the Brown et al. (1982) model of polarization of binary systems with eccentric orbits, Robert et al. (1992) estimated the average orbital inclination (i) of 114° and an eccentricity (e) of 0.39. They found that previous photopolarimetry, similarly analyzed, yielded a fairly narrow spread in these parameters, in spite of the differences in the actual polarization curves. However, because the photopolarimetry does not show strictly reproducible behaviour from season to season, it is clear that the polarization variability cannot be explained by binary effects alone. Furthermore, the medium-term stability of the variation, over time-scales much longer than the wind-flow time-scale, excludes wind inhomogeneities as a source of the secular variation.

An alternative explanation of the periodic spectroscopic, photometric, and polarimetric variability is rota-

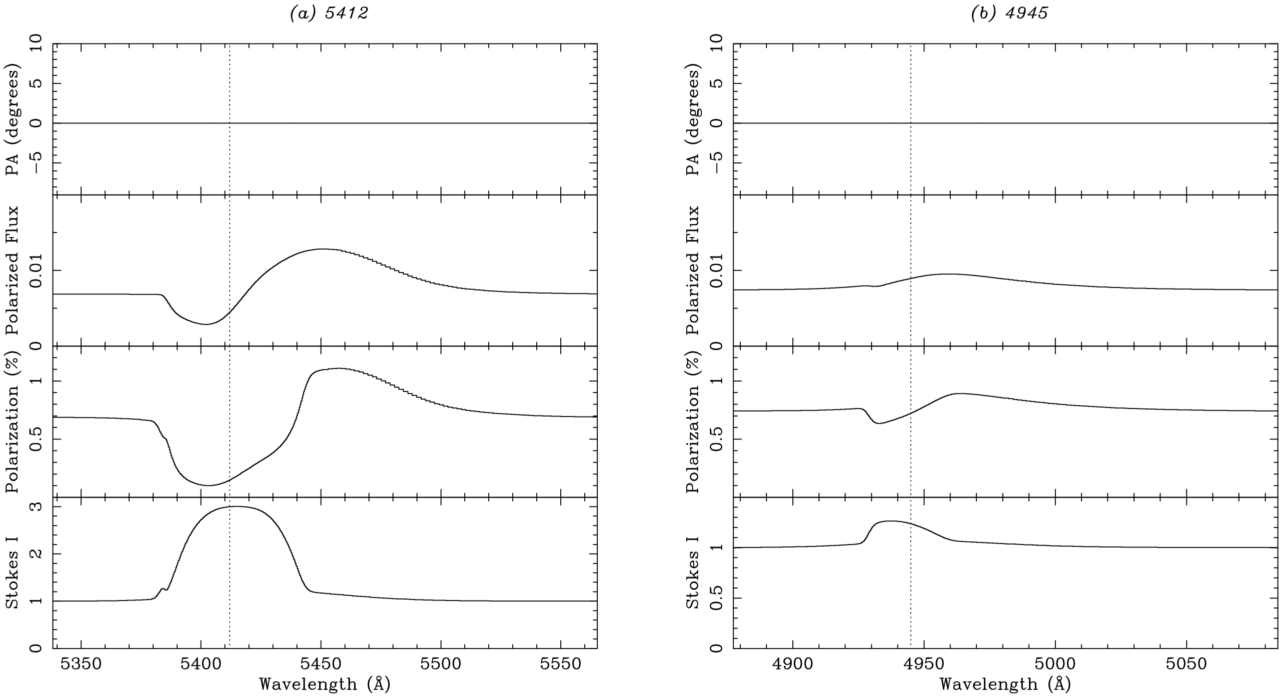

Figure 7. Model polarization spectra of the (*a*) He II $\lambda5412$ and (*b*) N V $\lambda4945$ emission lines. The dotted line shows the central wavelength of the line.

tional modulation. A specific form of this class of model, corotating interaction regions (CIRs), was invoked by St-Louis et al. (1995) as a possible explanation of the UV emission-line variability seen during the 16-d *IUE* 'MEGA' campaign. Although largely *ad hoc*, this model has the distinct advantage that epoch dependence of the variability can be introduced naturally, while preserving periodicity on shorter (rotational) timescales.

Further insight into the polarization variability may be gained by plotting published continuum measurements in the QU plane after subracting the ISP value previously derived (see Figure 8). It is immediately apparent that rather than being evenly distributed in the plane around the origin (the ISP value) the continuum polarizations are preferentially distributed in the $U < 0$ area, and there is some evidence that the distribution is slightly skewed to negative values of Q as well. The Robert et al. (1992) measurements have polarization magnitudes which are in general much smaller than those measured by D89, the Pine Bluff Observatory (PBO; see Table 5), and the AAT spectropolarimetric data presented here.

The skewed distribution of continuum polarization measurements is intriguing, since a simple CIR geometry (such as radial plumes) would be expected to produce an even distribution about the ISP value. The Robert et al. (1992) data (the open squares in Figure 8) encircle the ISP value, whereas the D89 measurements (filled squares) are scattered about a locus that passes close to the ISP, but extends much further into the $U < 0$ area. An increased amplitude of polarization variability requires either an increase in the electron-scattering depth in the envelope, or a change in the wind-geometry (this is true of both the CIR and binary models). Since the emission line flux in EZ CMa relatively stable (see Figure 1) it is unlikely that the mass-loss rate (and therefore the electron-depth) changes substantially from epoch-to-epoch, unless this is accompanied by a compensating change in the clumping factor. It is more plausible that changes in the polarization variability amplitude are caused by a geometrical redistribution of a constant wind outflow (for example the 'focusing' of a fraction of the wind into radial plumes). This scenario is broadly supported by photometric observations, which show epoch-to-epoch changes in the quasi-periodic light-curve, for example one substantial peak per 3.7d cycle in 1987–1988 to three smaller peaks per cycle in 1990 (see Robert et al. 1992).

In the following section we construct a simple, single-scattering polarization model for a rotationally modulated wind, to investigate its relevance to the observed behaviour of EZ CMa.

5.1 A 'toy' model

A spherical wind structure may be computed from the mass-loss rate, $\dot{M}$, and velocity law, $v(r)$, which combine to yield the radial density structure under the constraint of mass conservation:

$$\rho(r) = \frac{\dot{M}}{4\pi r^2 v(r)}. \tag{5}$$

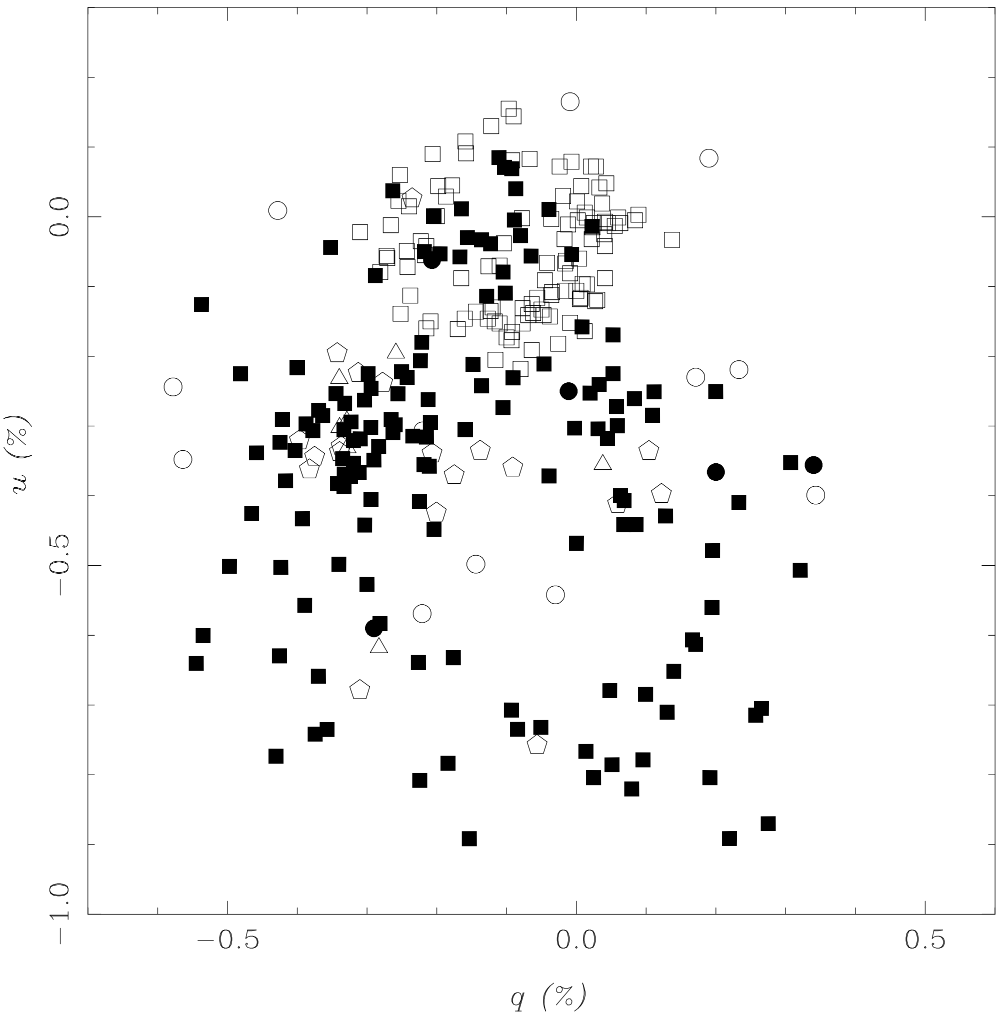

Figure 8. A compilation of continuum polarization measurements of EZ CMa published in the literature and plotted in the QU plane after subtraction of the interstellar polarization. The data are b-band observations by D89 (filled squares), b-band observations by Robert et al. (1992; open squares), integrated spectropolarimetry of SL90/SL91 (open triangles), B-band data from Pine Bluff Observatory (open pentagons), B-band data from Moffat & Piirola (1993; filled circles) and integrated spectropolarimetry from this publication (open circles).

We adopted a standard Castor & Lamers (1979) 'β law' to represent the radial velocity structure:

$$v(r) = v_0 + (v_\infty - v_0)(1 - r/R_*)^\beta, \tag{6}$$

where v_0 is a minimum velocity (required to avoid a singularity in Eq. 5), v_∞ is the terminal velocity, R_* is the core radius of the WR, and β is the acceleration parameter. If we assume a fully-ionized, pure-helium wind, then the electron density is given by

$$n_{\rm e}(r) = 2\frac{\rho(r)}{4m_h}, \tag{7}$$

where m_h is the mass of the hydrogen atom. We define the effective 'photospheric' radius of the WR star as the electron-scattering optical depth unity radius $R_{\tau=1}$, found from the integral equation

$$\int_\infty^{R_{\tau=1}} n_{\rm e}(r)\sigma_{\rm e} dr = 1 \tag{8}$$

where $\sigma_{\rm e}$ is the Thomson scattering cross-section. We assume that the flux emerging from the $R_{\tau=1}$ boundary is unpolarized.

We modify the symmetry of the wind by scaling up the density within selected volume elements, while normalizing the structure to ensure that the number of electrons (i.e., the mass-loss rate) is conserved between models:

$$\int n_{\rm e}(r,\theta,\phi) dV = \text{constant}. \tag{9}$$

Table 3. Emission line polarization measurements of EZ CMa. The wavelengths of the line (or complex) are given, along with the ionic species, and the ratio R.

λ (Å)	Species	R
	1991 Jan. 28	
5412	He II	$+0.22 \pm 0.03$
4945	N V	$+0.29 \pm 0.30$
4859	He II	$+0.22 \pm 0.04$
4686	He II	$+0.15 \pm 0.02$
4601–20	N V	$+0.01 \pm 0.03$
4542	He II	-0.15 ± 0.04
	1992 Jan. 29	
5412	He II	$+0.27 \pm 0.04$
4945	N V	$+0.25 \pm 0.26$
4859	He II	$+0.32 \pm 0.07$
4686	He II	$+0.15 \pm 0.02$
4601–20	N V	$+0.05 \pm 0.05$
4542	He II	-0.05 ± 0.04
	1992 March 11	
5412	He II	$+0.23 \pm 0.03$
5801–20	C IV	$+0.04 \pm 0.03$
5876	He I	$+0.00 \pm 0.05$
	1992 March 12	
5412	He II	$+0.25 \pm 0.03$
5801–20	C IV	-0.02 ± 0.04
5876	He I	-0.35 ± 0.25
	1992 March 17	
6560	He II	$+0.09 \pm 0.02$
6683+6678	He II/I	-0.35 ± 0.25
	1994 May 6	
6560	He II	$+0.14 \pm 0.02$
6683+6678	He II/I	$+0.02 \pm 0.10$
	1994 May 7	
6560	He II	$+0.08 \pm 0.02$
6683+6678	He II/I	$+0.24 \pm 0.24$
	1994 May 8	
6560	He II	$+0.03 \pm 0.02$
6683+6678	He II/I	-0.05 ± 0.10
	1994 May 9	
6560	He II	$+0.16 \pm 0.04$
6683+6678	He II/I	$+0.00 \pm 0.10$
	1995 Apr. 28	
4945	N V	$+0.25 \pm 0.24$
4859	He II	$+0.38 \pm 0.15$
4686	He II	$+0.25 \pm 0.01$
4601–20	N V	$+0.22 \pm 0.04$
4542	He II	$+0.10 \pm 0.04$
6560	He II	$+0.23 \pm 0.04$
6683+6678	He II/I	-0.29 ± 0.15
	1995 Apr. 29	
6560	He II	$+0.08 \pm 0.02$
6683+6678	He II/I	-0.02 ± 0.09
	1997 Aug 9	
6560	He II	$+0.08 \pm 0.02$
6683+6678	He II/I	-0.02 ± 0.10

The continuum polarization at observer direction vector $\hat{\mathbf{v}}$ may be computed from the wind structure using a similar approach to Brown & McLean (1977). For a volume element dV with position vector $\mathbf{r}$ and direction vector $\hat{\mathbf{r}}$, the scattering-angle χ is given by

$$\cos\chi = \hat{\mathbf{v}} \cdot \hat{\mathbf{r}}, \qquad (10)$$

Table 4. Mean average values of R for each line computed from the data in Table 3.

λ (Å)	Species	R
4542	He II	-0.04 ± 0.02
4601–20	N V	$+0.09 \pm 0.02$
4859	He II	$+0.31 \pm 0.06$
4945	N V	$+0.26 \pm 0.15$
5412	He II	$+0.24 \pm 0.01$
5801–20	C IV	$+0.01 \pm 0.02$
5876	He I	-0.18 ± 0.13
6560	He II	$+0.11 \pm 0.01$
6683+6678	He I/II	-0.06 ± 0.05

Table 5. Simulated B-band data of EZ CMa obtained by using the HPOL spectropolarimeter at the Pine Bluff Observatory.

Date	q (%)	u (%)	σ (%)
1989 Mar. 08	-0.0017	-0.5654	0.0098
1990 Feb. 05	$+0.0198$	-0.5889	0.0073
1990 Feb. 20	$+0.0555$	-0.5823	0.0066
1990 Feb. 21	$+0.0824$	-0.4688	0.0087
1990 Deb. 25	$+0.1174$	-0.4829	0.0054
1990 Feb. 28	$+0.0124$	-0.6071	0.0134
1990 Mar. 02	$+0.4543$	-0.6566	0.0073
1990 Mar. 03	$+0.0846$	-0.9235	0.0087
1990 Nov. 29	$+0.2198$	-0.6154	0.0075
1990 Nov. 30	$+0.0521$	-0.4404	0.0088
1990 Dec. 07	$+0.0579$	-0.5742	0.0163
1990 Dec. 14	$+0.2573$	-0.5804	0.0128
1991 Jan. 02	$+0.3039$	-0.6044	0.0093
1991 Jan. 10	$+0.1942$	-0.6690	0.0086
1991 Jan. 22	$+0.1882$	-0.5841	0.0060
1991 Jan. 28	$+0.4990$	-0.5806	0.0244
1992 Mar. 13	$+0.5169$	-0.6423	0.0204
1992 Mar. 18	$+0.3386$	-1.0023	0.0213
1994 Dec. 02	$+0.1595$	-0.2185	0.0087

while the normal to the scattering-plane is $\hat{\mathbf{n}} = \hat{\mathbf{v}} \times \hat{\mathbf{r}}$. The intensity of scattered light is then

$$\begin{aligned} dI &= I_0 \frac{3\sigma_{\rm e}}{16\pi r^2} n_{\rm e}(r,\theta,\phi)(1+\cos^2\chi)dV, \\ dQ &= I_0 f \frac{3\sigma_{\rm e}}{16\pi r^2} n_{\rm e}(r,\theta,\phi)(1-\cos^2\chi)dV, \qquad (11) \\ dU &= 0, \end{aligned}$$

where I_0 is the emergent intensity and f is the finite-disk depolarization factor,

$$f = \sqrt{(1 - R^2_{\tau=1}/r^2)} \qquad (12)$$

(Cassinelli, Nordsieck & Murison 1987).

The polarization in the observer's frame is then given by rotating dI, dQ, dU by twice the angle between the observer's north $\hat{\mathbf{N}}$ and the normal to the scattering plane (measured over the observer's east, $\hat{\mathbf{E}}$),

$$\tan\eta = \hat{\mathbf{N}} \cdot \hat{\mathbf{n}} / \hat{\mathbf{E}} \cdot \hat{\mathbf{n}} \qquad (13)$$

so

$$dQ' = dQ\cos 2\eta + dU \sin 2\eta$$

Table 6. Parameters for the model of EZ CMa.

Parameter	Value
Core temperature, T_*	74 kK
Core radius, R_*	2.8 $R_\odot$
$\log(L_*/L_\odot)$	5.32
Mass-loss rate, $\log(\dot{M}/M_\odot)$	-4.06
Terminal velocity, v_∞	1700 $\mathrm{km\,s^{-1}}$
Velocity law index, β	1.3

$$dU' \quad = \quad dU \cos 2\eta - dQ \sin 2\eta \tag{14}$$

The components of the continuum polarization vector are simply the sums of dI, dQ' and dU' over the wind volume. However, some of the wind is occulted by the $R_{\tau=1}$ boundary: the angle subtended at the volume element by the observer direction and the centre of the WR star is $\alpha = \cos^{-1} -\hat{\mathbf{r}} \cdot \hat{\mathbf{v}}$, so if

$$|\mathbf{r}| \sin \alpha < R_{\tau=1} \tag{15}$$

then the scattered flux is occulted by the $R_{\tau=1}$ surface and this volume element is not included in the integration.

We tested our implementation of these equations against the formulation given by Fox (1991) and found excellent agreement.

5.2 Some illustrative computations

The physical parameters of EZ CMa were taken from the tailored model presented by Crowther (1994) and are listed in Table 6. A very simple 'orange segment' wind structure was employed, with n high-density sectors of varying width and density-contrast factor. The inclination of EZ CMa (whether the binary orbit inclination or the inclination of the rotation axis) is evidently not very close to 90°, since in the high-inclination case the polarimetric variations would follow a linear track in QU space. The stability of the emission-line shape (see Figure 1) implies that $\rho(v)$ must be roughly constant in the azimuthal direction, although changes in the velocity law (which we do not model) may allow changes in the $\rho(r)$ structure without affecting the emission-line morphology. We arbitrarily adopt a factor 2 density contrast between low- and high-density sectors, although the emission measure ($n_e^2 V$) of the high-density regions must be small compared to the emission measure of the entire wind volume.

When occultation is ignored, a wind structure of $n(> 2)$ high-density sectors of equal angular width evenly distributed in azimuth will produce no nett polarization. Occultation of the scattering volume immediately behind the $R_{\tau=1}$ sphere will break this symmetry, and a small polarization will result. Figure 9 shows the polarization light-curves of four models all viewed at an inclination of 30°. It is apparent that the models with $n > 2$ produce a polarization signal that is strongest in the n^{th} harmonic of the period, and also produce a peak-to-peak variation in polarization that is typically 0.1–0.2%. Both the $n = 1$ and $n = 2$ models produce most power in the second harmonic of the period, with the largest peak-to-peak variation occurring in the $n = 2$ model, since the polarization vectors produced by the two segments (ignoring occultation) are the same and vary identically as a function of phase.

Although very simple, these illustrative models allow us to draw conclusions about the possible azimuthal structure of the wind of EZ CMa. Structures with many ($n > 2$) similar high-density segments that are roughly evenly distributed in azimuth will produce neither the peak-to-peak polarization amplitude that is observed, nor the strong power in the second harmonic. Wind structures with one or two high-density sectors (which need not be evenly distributed in azimuth) are capable of producing the peak-to-peak amplitude of the polarization variation.

These toy models cannot reproduce the shape of the polarized light-curve of EZ CMa since the minima in the Stokes parameters are separated by 0.4 in phase, whereas the one- or two-segment models have minima separated by 0.5. However, we suggest that they do serve the purpose of demonstrating that rotational modulation provides a plausible alternative to binary motion as an explanation for periodic polarimetric variability. Unfortunately, unlike the binary-system model, we do not have a firm physical basis for extending the rotation model beyond the illustrative calcultions given here, but it is clear that only a small number of large-scale structures is consistent with observations.

6 SUMMARY AND DISCUSSION

Previous time-series observations have shown that the continuum polarization of EZ CMa varies with a 3.7-d period, a period also associated with emission-line variations. The form of the photopolarimetric curve varies over time-scales of months, and does not show the sinusoidal shape produced by light-scattering in a close binary with a circular orbit. Observations of short-period WR+O star binaries show polarized-light curves which are stable over many years. Our continuum spectropolarimetry undersamples, but is broadly consistent with, the photopolarimetry (particularly the 1994 observations over consecutive nights).

The amplitude of continuum-polarization variability is about 0.8%, while the PA of the intrinsic polarization varies over a whole quadrant. The lines clearly depolarize, and our 1994 results, in particular, allow a precise ISP determination. This in turn provides the first reliable measurements of the intrinsic polarization of EZ CMa, which of course is the quantity required to constrain possible system geometries.

The intrinsic line polarization profiles show a P-Cygni structure in polarized flux, which is qualitatively matched by the radiative-transfer models, although the electron-scattered red-wings are too strong in the synthetic profiles. Measurements of the polarized-line flux relative to the line intensity show some evidence for the ionization stratification predicted by the Standard Model.

What is the wind geometry of EZ CMa? Clearly the structure is variable over a time-scale of months but stable over a time-scale of days, as indicated by the line-profile variations, the photometry, and the broad-band polarimetry. A 3.7d period is consistently recovered from the observations, suggesting that the variability may have its root in stellar rotation. Inclusion of centrifugal terms in canonical radiation-driven wind theory indicates that rapid rotation will lead to

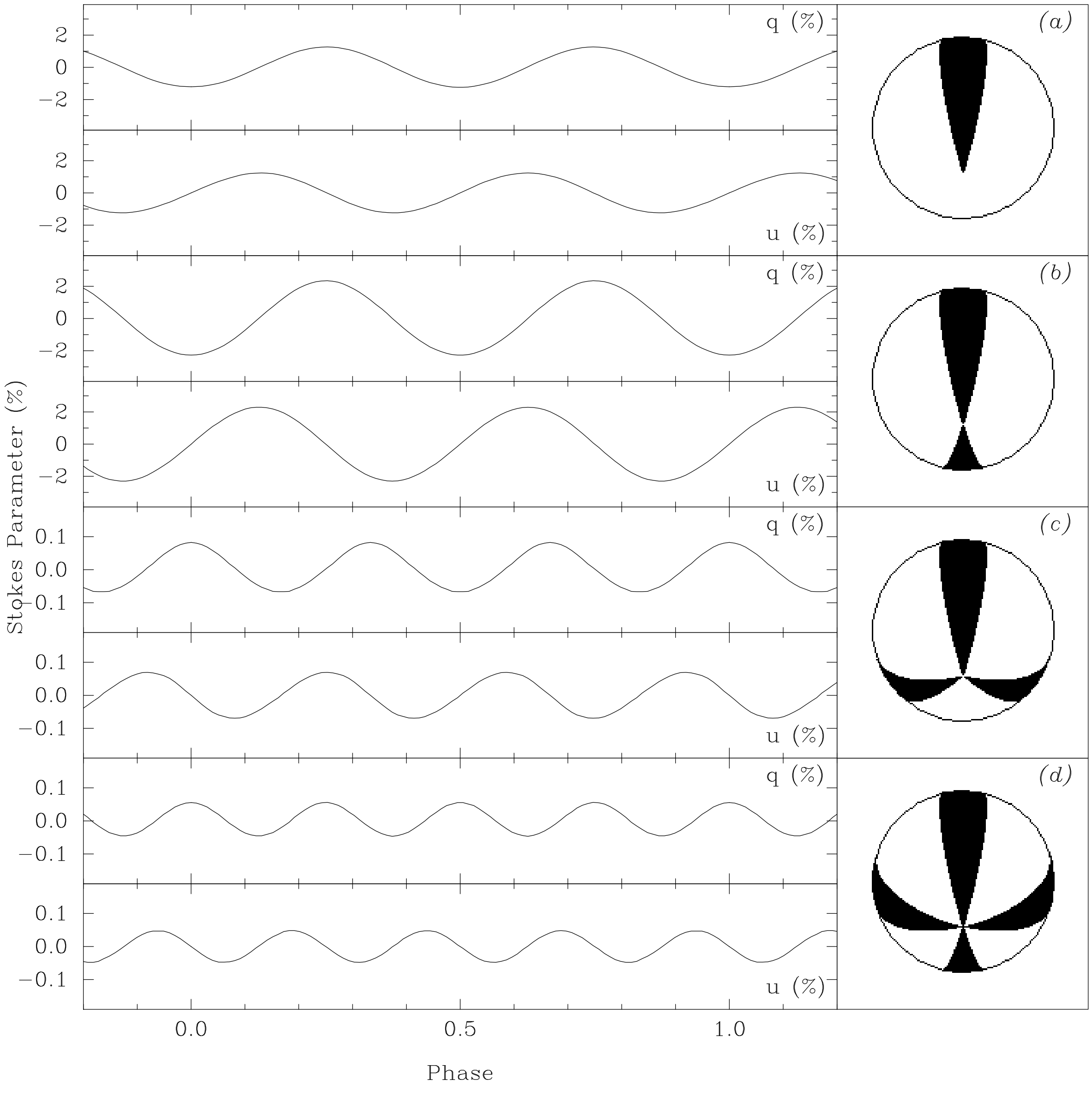

Figure 9. Illustrative models of an 'orange segment' wind. The left-hand panels show the percentage normalized Stokes q and u parameters as a function of phase. The right-hand panels illustrate the wind geometry at phase zero, with the black areas representing the high-density regions. Model *(a)* has one 30° high-density segment, *(b)* has two segments, *(c)* three segments, and *(d)* four segments.

enhanced mass-loss at the equator, and if the variability is neglected such axisymmetric structure model may reproduce the observed continuum polarization magnitude with equator:pole density ratios of 3. We have shown however that such models produce too much polarized line flux (§ 4.2), and reconciling the models with the observations would require a substantial change in the electron-scattering depth to the line formation region, by increasing the clumping factor (which would degrade the agreement of the red-wing of the line intensity with the model).

Of course such an axisymmetric structure cannot reproduce the wind variablity that is observed, and we must turn to more complex (and necessarily more *ad hoc*) models. The co-rotating interaction region (CIR) model discussed in sections 5 and 5.1 provides an attractive alternative. The 'toy' model detailed in §5.1 shows that rotational modulation of a small number of large-scale structures is broadly consistent with the observations. These structures must be variable over a timescale of months to accord with the seasonal variability observed photopolarimetrically. Since this timescale is very much greater than the wind-flow timescale (~hours), these structures must have a deep-seated origin.

A significant problem with the CIR model is encapsulated in Figure 8, in that a CIR geometry will produce continuum polarization vectors that are approximately evenly distributed about, and a constant magnitude from, the ISP value. The bias in the QU distribution plot indicates a prefered direction (on the plane of the sky) of wind variability, while the different distances from the ISP suggests that the $\tau_{es} = 1$ electron-scattering surface is radially variable. This behaviour could result from a combination of wind flattening (to provide a prefered direction) and co-rotating regions (producing the stochastic variability), with the seasonal variability resulting from changes in the disk structure.

The most obvious mechanism for producing these large-scale structures is a global, co-rotating magnetic field. Although EZ CMa shows no circular polarization (e.g. D89) indicative of cyclotron emission in a large-scale magnetic field, a local field strength of only 200G might be enough to significantly influence the structure of the outflow (Friend & MacGregor 1984). The spectropolarimetric data presented here provide a strong test of future magnetically-distorted wind models.

ACKNOWLEDGEMENTS

We are grateful to Paul Crowther for supplying the EZ CMa parameters. The AAT observations benefitted from the excellent support of the AAO staff. The PBO observations were gathered with the HPOL spectropolarimeter by a team of observers headed by K.H. Nordsieck, whose conributions to this project we wish to acknowledge here. We obtained the reduced data through the HPOL webpage at http://www.sal.wisc.edu/HPOL/ maintained by M.R. Meade and B.L. Babler. Funding for PBO and AAT observations by RS-L was provided in support of the Astro space shuttle missions through NASA grants number NAS5026777 to the University of Wisconsin and NAG8-1073 to the University of Pittsburgh.

REFERENCES

Antokhin I., Bertrand J.-F., Lamontagne R., Moffat A.F.J, 1994, AJ, 107, 2179
Brown J.C., McLean I.S., 1977, A&A, 57, 141
Brown J.C., Aspin C., Simmons J.F.L., McLean I.S., 1982, MNRAS, 198, 787
Cassinelli J.P., Nordsieck K.H., Murison M.A., 1987, ApJ, 317, 290
Castor J.I., Lamers H.G.J.L.M., 1979, ApJS, 39, 481
Cherepaschuk A.M., 1981, MNRAS, 194, 755
Cropper M., Bailey J., McCowage J., Cannon R.D., Couch W.J., Walsh J.R., Strade J.O., Freeman F., 1988, MNRAS, 231, 695
Crowther P.A., 1994, PhD Thesis, University of London
Drissen L., Robert C., Lamontagne R., Moffat A.F.J., St-Louis N., van Weerden N., van Genderen A.M., 1989, ApJ, 343, 426 (D89)
Duijsens M.F.J., van der Hucht K.A., van Genderen A.M., Schwarz H.E., Linders H.P.J., Kolkman O.M., 1996, A&AS, 119, 37
Fox G.K., 1991, ApJ, 379, 663
Friend D.B., MacGregor K.B., 1984, ApJ, 282, 591
Harries T.J., 1996, Starlink User Note, No. 204
Harries T.J., Howarth I.D., 1996, A&AS, 119, 61
Hillier D.J., 1987a, ApJS, 63, 947
Hillier D.J., 1987b, ApJS, 63, 965
Hillier D.J., 1988, ApJ, 347, 392
Hillier D.J., 1996, A&A, 308, 521
Hillier D.J., Miller D.L., 1998, ApJ, 496, 407
Lamontagne R., Moffat A.F.J., Lamarre A., 1986, AJ, 91, 925
McLean I.S., Coyne G.V., Frecker J.E., Serkowski K., 1979, ApJ, 228, 802 (MC79)
McLean I.S., 1980, ApJ, 236, L149
Moffat A.F.J., Piirola V.,1993, ApJ, 413, 724
Morel T., St-Louis N., Marchenko S.V., 1997, ApJ, 489, 1004
Poeckert R., Malborough J.M., 1978, ApJ, 220, 940
Robert C., Moffat A.F.J., Seggewiss W., 1991, in K.A. van der Hucht, B. Hidayat (eds), IAU Symp. 143: Wolf-Rayet Stars and Interrelations with Other Massive Stars in Galaxies, Kluwer (Dordrecht), p.147
Robert C., Moffatt A.F.J., Drissen L., Lamontagne R., Seggewiss W., Niemala V.S., Cerruti M.A., Barrett P., Bailey J., Garcia J., Tapia S., 1992, ApJ, 397, 277
Schulte-Ladbeck R.E., Nordsieck K.H., Nook M.A., Magalhães A.M., Taylor M., Bjorkman K.S., Anderson C.M. 1990, ApJ, 365, L19 (SL90)
Schulte-Ladbeck R.E., Nordsieck K.H., Nook M.A., Magalhães A.M., Taylor M., Bjorkman K.S., Anderson C.M. 1991, ApJ, 382, 301 (SL91)
Schulte-Ladbeck R.E., Nordsieck K.H., Taylor M., Bjorkman K.S., Magalhães A.M., Wolff M.J. 1992, ApJ, 387, 347
Serkowski K., 1973, in IAU Symp. 52: Interstellar Dust and Related Topics, J.M. Greenburg & D.S. Hayes (eds), Reidel (Dordrecht), p. 145
Serkowski K., Mathewson,D.S., Ford V.I., 1975, ApJ, 196, 261
Shortridge K., Meyerdierks H., Currie M., Clayton M., 1996, Starlink User Note (Rutherford Appleton Laboratory), no. 86
Skinner S.L., Itoh M., Nagase F., 1997, NewA, 3, 37
Stevens I.R., Willis A.J., 1988, MNRAS, 234, 783
St-Louis N., Howarth I.D., Willis A.J., Stickland D.J., Smith L.J., Conti P.S., Garmany C.D., 1993, A&A, 267, 447
St-Louis N., Dalton M.J., Marchenko S.V., Moffat A.F.J., Willis A.J., 1995, ApJ, 452, L57
van der Hucht K.A., Conti P.S., Lundström I., Stenholm B., 1981, Space Sci Rev, 28, 227
van Genderen A.M., van der Hucht K.A., Steemers W.J.G., 1987, A&A, 185, 131
Willis A.J., Howarth I.D., Smith L.J., Garmany C.D., Conti P.S., 1989, A&A, 77, 269